Journal of Molecular Graphics and Modelling 65 (2016) 43–60

Contents lists available at ScienceDirect

Journal of Molecular Graphics and Modelling

journal homepage: www.elsevier.com/locate/JMGM

Development of an accurate molecular mechanics model for buckling behavior of multi-walled carbon nanotubes under axial compression

B. Safaei [a,*], P. Naseradinmousavi [b], A. Rahmani [c]

[a] Young Researchers and Elite Club, Electronic Branch, Islamic Azad University, Tehran, Iran
[b] Department of Mechanical Engineering, San Diego State University (SDSU), San Diego, CA 92115, USA
[c] Department of Mechanical Engineering, Ajabshir Branch, Islamic Azad University, Ajabshir, Iran

ARTICLE INFO

Article history:
Received 7 December 2015
Accepted 6 February 2016
Available online 15 February 2016

Keywords:
Nanomechanics
Carbon nanotubes
Axial buckling
Molecular mechanics model
Density functional theory

ABSTRACT

In the present paper, an analytical solution based on a molecular mechanics model is developed to evaluate the elastic critical axial buckling strain of chiral multi-walled carbon nanotubes (MWCNTs). To this end, the total potential energy of the system is calculated with the consideration of the both bond stretching and bond angular variations. Density functional theory (DFT) in the form of generalized gradient approximation (GGA) is implemented to evaluate force constants used in the molecular mechanics model. After that, based on the principle of molecular mechanics, explicit expressions are proposed to obtain elastic surface Young's modulus and Poisson's ratio of the single-walled carbon nanotubes corresponding to different types of chirality. Selected numerical results are presented to indicate the influence of the type of chirality, tube diameter, and number of tube walls in detailed. An excellent agreement is found between the present numerical results and those found in the literature which confirms the validity as well as the accuracy of the present closed-form solution. It is found that the value of critical axial buckling strain exhibit significant dependency on the type of chirality and number of tube walls.

1. Introduction

Carbon nanotubes (CNTs) are one of the stable families of carbon structures which have been attracted much attention of the scientific community research through their remarkable physical, electrical, and mechanical properties [1–4]. As the size of the CNTs is at the nano scale there are some difficulties in the experimental methods to investigate the behaviors of them that causes theoretical analyses of nanostructures are becoming increasingly important.

Modified continuum models have been one of the applied analytical methods in nano mechanics due to their computational efficiency and the capability to produce accurate results which are comparable to those of atomistic models. The application of nonlocal continuum mechanics allowing for the small scale effects to the vibrational analysis of nanomaterials has been recommended by many research workers [5–15]. However, continuum based models have at least two shortcoming in their analyses. At first, there is not any consensus on the correct value of effective thickness used in the calculations. Li and Chou [16] extracted the effective thickness of carbon nanotubes equal to 0.066 nm through comparison of the molecular dynamics simulation results with the ones of continuum model. Chang et al. [17] proposed an effective thickness of 0.0617 nm on the basis of study on the carbon nanotube deformation. The value of 0.71 nm was obtained for effective thickness by Fang et al. [18] with a tight bonding molecular dynamics. Moreover, in many researches the value of spacing of graphite (0.34 nm) has been utilized in the analyses. Another deficiency of the continuum mechanics is that it has not the capability to incorporate the effect of chirality into account because of disregarding the discrete nature of atomic structures.

Molecular mechanics model is another efficient type of computational methods which is considered as a powerful tool to investigate the mechanical responses of nano structures analytically without the shortcomings mentioned before. Zhang et al. [19] presented an analytical model based on molecular mechanics approach to derive explicit expressions for elastic modulus and Poisson's ratio of SWCNTs as a function of the nanotube diameter. On the basis of molecular mechanics model, Cornwell and Wille [20] obtained analytical solutions for the critical axial buckling strain of achiral SWCNTs under axial compression and showed that zigzag tubes are more stable than armchair

* Corresponding author. Fax: +98 413 657 2500.
E-mail addresses: stu.bsafaei@iaut.ac.ir, babak.safaei.me@gmail.com (B. Safaei).

http://dx.doi.org/10.1016/j.jmgm.2016.02.001
1093-3263/

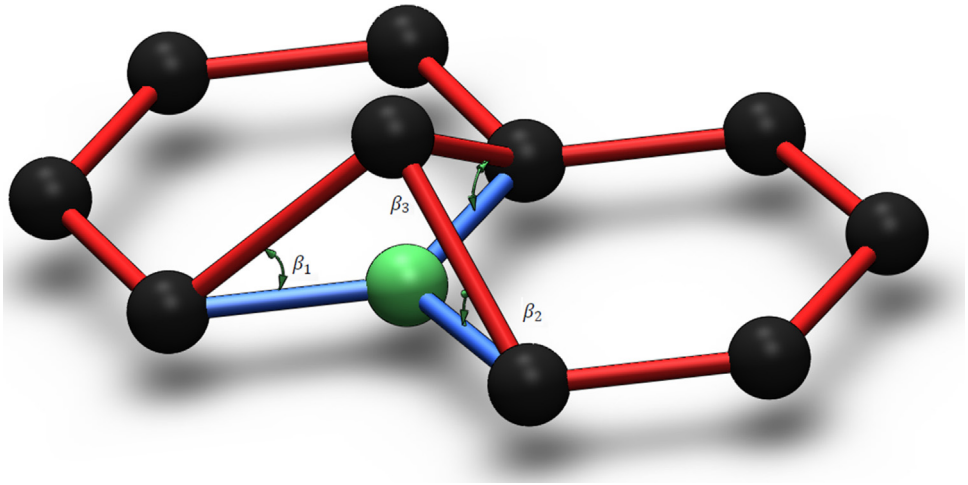

Fig. 1. Definition of the inversion angle components.

ones with the same diameter. Wang et al. [21] calculated the surface Young's moduli of SWCNTs with dissimilar diameters as well as chiral angles using molecular mechanics simulation. A finite element model of SWCNTs based on molecular mechanics theory was proposed by Ni et al. [22] to evaluate Young's modulus, ultimate strength and strain of SWCNTs. Korobeynikov et al. [23] used the molecular mechanics method based on the modified Morse force field to determine the critical buckling parameters and postbuckling deformation of SWCNTs twisted at edges. Kinoshita et al. [24] investigated the axial compressive stress–strain relationships and deformation processes of wavy SWCNTs with multiple Stone–Wales defects using molecular mechanics simulations with the adaptive intermolecular reactive empirical bond-order potential. Ansari et al. [25] described the axial buckling behavior of chiral SWCNTs using a combined continuum-atomistic approach. To this end, the nonlocal Flugge shell theory is implemented into which the nonlocal elasticity of Eringen incorporated. Molecular mechanics is used in conjunction with density functional theory (DFT) to precisely extract the effective in-plane and bending stiffnesses and Poisson's ratio used in the developed nonlocal Flugge shell model.

In the current study, axial buckling characteristics of MWCNTs with different types of chirality and values of tube diameter and number of tube wall are investigated using molecular mechanics modeling. Density functional theory (DFT) in conjunction with the generalized gradient approximation (GGA) is implemented to obtain the relevant elastic constants of the nanotubes. Closed-form analytical solution is presented to evaluate the critical axial buckling strain of the nanotubes relevant to various amounts of chiral angles. It is observed that the present tight-binding molecular mechanics model has the capability to predict axial buckling behavior of MWCNTs accurately as well as quickly.

2. Molecular mechanics model

2.1. Total potential energy

The total potential energy, E_t, in the empirical force field method of molecular mechanics, can be stated as the sum of several energies due to valence of bonded interactions or bonded and non-bonded interactions

$$E_t = U_\rho + U_\theta + U_\omega + U_\tau + U_{vdw} + U_{es} \tag{1}$$

in which U_ρ, U_θ, U_ω, and U_τ are energies associated with bond stretching, bond angle variation, bond inversion,and torsion, respectively; U_{vdw} and U_{es} are also associated with van der Waals and electrostatic interactions (see Refs. [26,27–30]), respectively.

Depending on the particular materials and loading conditions considered, different functional forms might be utilized for these energy terms. For the present buckling problem of carbon nanotubes, the terms U_ρ, U_θ, U_ω and U_{vdw} are expected to be significant in the total potential energy of the system. As Hooke's law has proven to be efficient and precise enough to describe the behavior of atoms under small deformation [31], it is frequently employed to characterize the interactions between bound atoms in the system, therefore, Eq. (1) may be written in the form

$$E_t = \sum \frac{1}{2} K_\rho (dr)^2 + \sum \frac{1}{2} C_\theta \left(d\theta\right)^2 + \sum \frac{1}{2} C_\omega (dC)^2 + \sum \frac{1}{2} K_{vdw} (ds)^2 \tag{2}$$

where dr, dθ, dC and dS are the bond elongation, bond angle variance, the change of space between two atoms and the jump in deflection at the atomic position, respectively. The average inversion angle β is

$$\beta = \frac{1}{3}\left(\beta_1 + \beta_2 + \beta_3\right) \tag{3}$$

here, β_1, β_2 and β_3 are illustrated in Fig. 1. The force constants K_ρ, C_θ and C_ω associated, respectively, with energies of bond stretching, bond angle variation and bond inversion can be determined theoretically or experimentally.

As there are three bond lengths $r_{ij1}, r_{ij2}, r_{ij3}$ and three bond angles $\theta_{ij1}, \theta_{ij2}, \theta_{ij3}$ associated with an atom indexed by ij in a carbon nanotube (Fig. 2), one can re-write Eq. (2) in a more specific form, i.e.

$$E_t = \frac{1}{2}\sum_{ij}\frac{1}{2}K_\rho\sum_k\left(dr_{ijk}\right)^2 + \sum_{ij}\frac{1}{2}C_\theta\sum_k\left(d\theta_{ijk}\right)^2 + \sum_{ij}\frac{1}{2}C_\omega\left(\frac{1}{3}\sum_k\beta_{ijk}\right)^2 + \frac{1}{2}\sum_i\frac{1}{2}K_v\left[\left(d\omega_{ij}^+\right)^2 + \left(d\omega_{ij}^-\right)^2\right] \tag{4}$$

here the subscript $k = 1, 2, 3$. Besides, it should be remarked that the constant coefficient 1/2 of the first term and fourth terms in Eq. (4) is to ensure that bond stretching energy is considered only once. ω_{ij} is the radial displacement of atom ij, and $d\omega^+$ ($d\omega^-$) represents the jump in the deflection between the wall on which atom ij located and its inner (outer) adjacent wall. It should be noted that $d\omega^+$ ($d\omega^-$) should be set to be zero for the innermost (outermost) wall.

2.2. Axisymmetric buckling of chiral single-walled carbon nanotubes

The structure of a single-walled carbon nanotube is often characterized by a pair of integers (n,m), representing its helicity [32]. When an axially compressed single-walled carbon nanotube is considered, the energy term in Eq. (4) associated with the intertube van de Waals interaction can be neglected. For an undeformed (n,m) larihc carbon nanotubes, one have the following geometrical parameters

$$r_{ij1} = r_{ij2} = r_{ij3} = r_0 \tag{5}$$

$$\beta_{ij1} = \frac{\pi}{2\sqrt{n^2+nm+m^2}}\cos(\phi_1) \tag{6-a}$$

$$\beta_{ij2} = \frac{\pi}{2\sqrt{n^2+nm+m^2}}\cos\left(\frac{\pi}{3}-\phi_1\right) \tag{6-b}$$

$$\beta_{ij3} = \frac{\pi}{2\sqrt{n^2+nm+m^2}}\cos\left(\frac{\pi}{3}+\phi_1\right) \tag{6-c}$$

$$\theta_{ij1} = \arccos\left(\sin(\phi_2)\sin(\phi_3)\cos\left(\beta_{ij1}\right) + \cos(\phi_2)\cos(\phi_3)\right)\, i, j, k = 1, 2, 3; i \neq j \neq k. \tag{7-a}$$

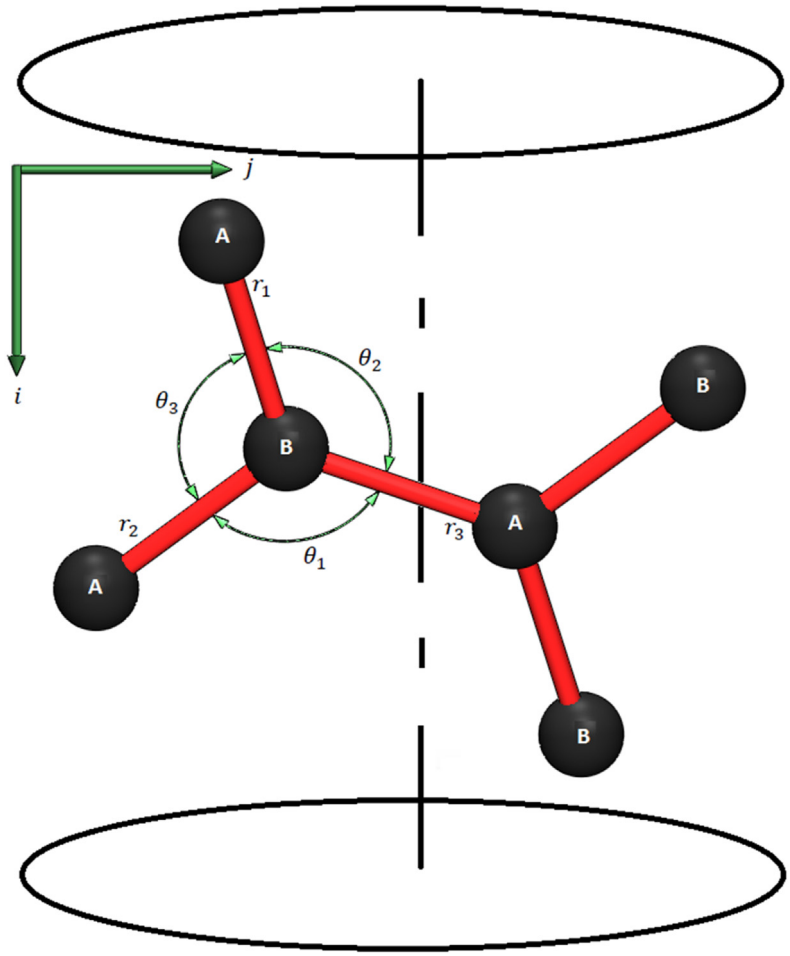

Fig. 2. Definition for atom position of type A and B in a chiral tube.

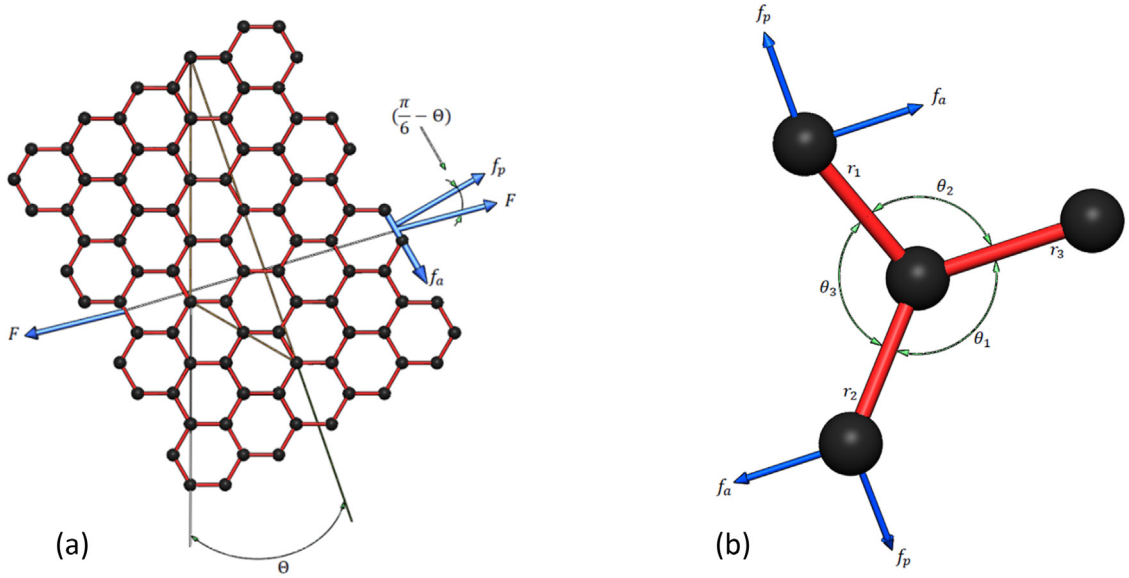

Fig. 3. Single-walled carbon nanotube under loading (a) decomposing of acting force (b) force distribution in bonds r_1 and r_2.

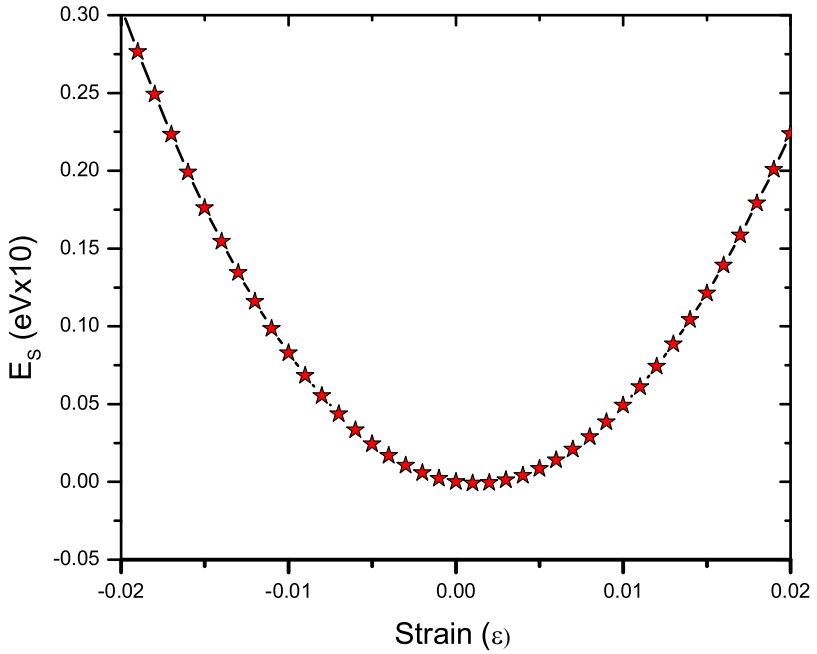

Fig. 4. Variation of the strain energy E_s with strain for grapheme.

$$\theta_{ij2} = \arccos\left(\sin(\phi_3)\sin(\phi_1)\cos\left(\beta_{ij2}\right) + \cos(\phi_3)\cos(\phi_1)\right) \tag{7-b}$$

$$\theta_{ij3} = \arccos\left(\sin(\phi_1)\sin(\phi_2)\cos\left(\beta_{ij3}\right) + \cos(\phi_1)\cos(\phi_2)\right) \tag{7-c}$$

where

$$\phi_1 = \arccos\left(\frac{2n+m}{2\sqrt{n^2+nm+m^2}}\right) \tag{8-a}$$

$$\phi_2 = \frac{4\pi}{3} + \phi_1 \tag{8-b}$$

$$\phi_3 = \frac{2\pi}{3} + \phi_1 \tag{8-c}$$

where r_{ij}, θ_{ij} and β_{ij} are bond length, bond angle and inversion angle of the atom ij, respectively. A carbon nanotube under compression tends to buckle when its axial strain exceeds the critical compressive strain, ε_0. Prior to buckling, the variation of bond length, bond angle and inversion angle from equilibrium values are obtained as follows.

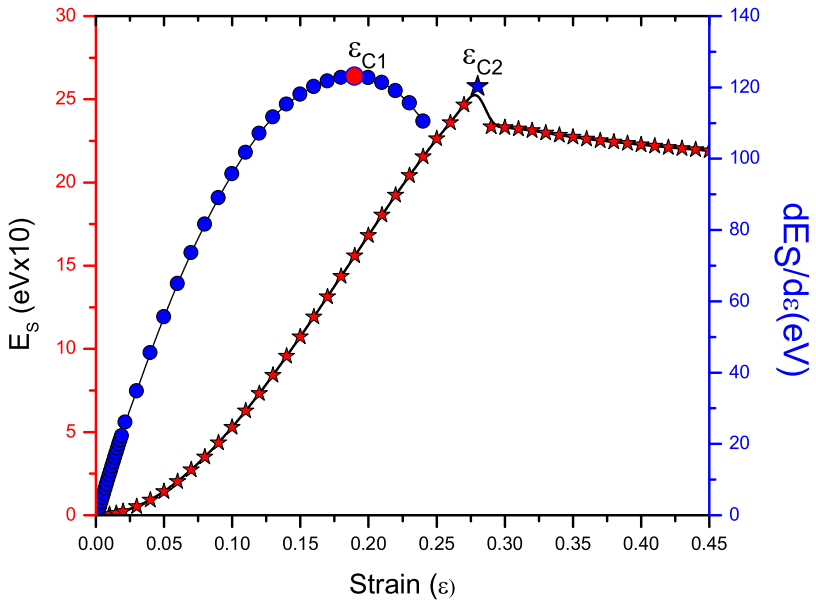

Fig. 5. Variation of the strain energy E_s and its derivative with strain of BN sheet. The strains corresponding to two critical points in the elastic range are indicated by ε_{C_1} and ε_{C_2}.

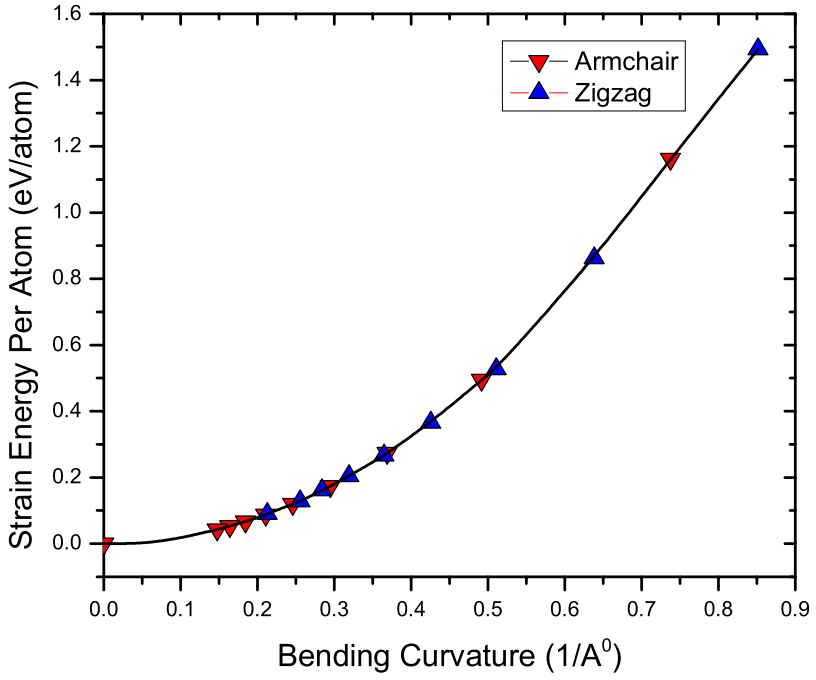

Fig. 6. Strain energy relative to planar boron-nitride for fully relaxed nanotubes of varying radius plotted vs a quadratic approximation of the bending energy with the flexural modulus predicted by the DFT.

Similar to those in Fig. 3 [33], the axial force F acting on a chiral single-walled CNT can be decomposed into f_p perpendicular to the bond r_3 and f_a along the bond r_3. The geometrical relationships between the two forces are given by

$$f_p = F\cos\left(\frac{\pi}{6} - \Theta\right) \tag{9}$$

$$f_a = F\sin\left(\frac{\pi}{6} - \Theta\right) \tag{10}$$

where the chiral angle Θ, is given by the expression

$$\Theta = \arccos\left(\frac{(2n+m)}{2\sqrt{\left(n^2+nm+m^2\right)}}\right) \tag{11}$$

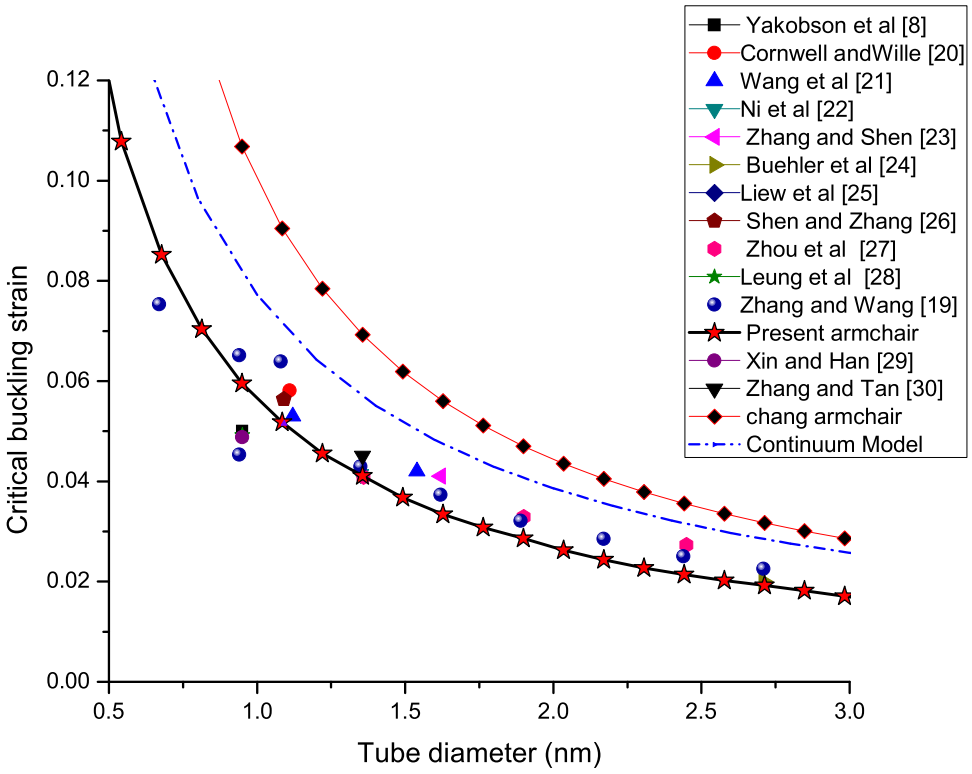

Fig. 7. Critical buckling strain versus tube diameter.

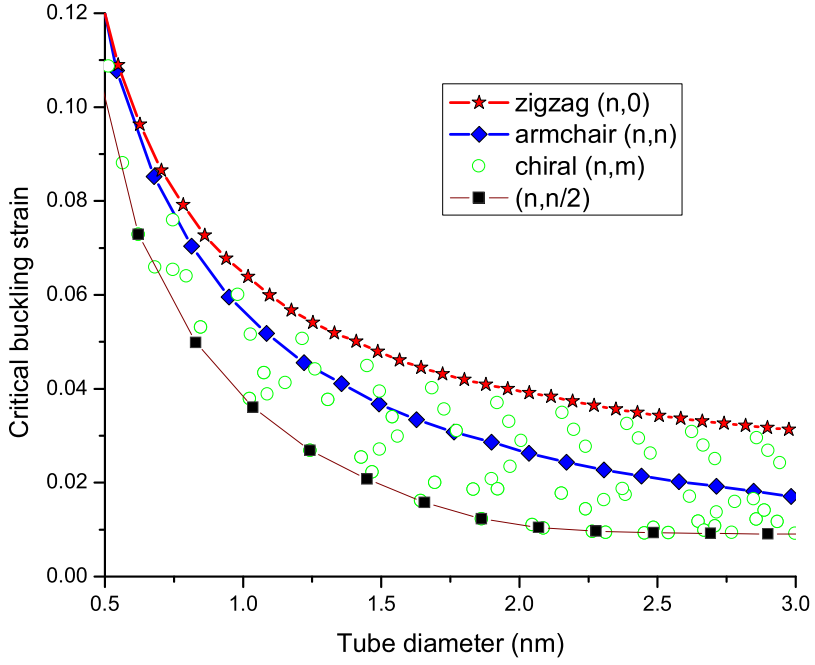

Fig. 8. Critical buckling strain versus tube diameter.

With reference to Fig. 5 from the force equilibrium

$$f_{\mathrm{p}} \sin\left(\frac{\theta_3}{2}\right) - f_{\mathrm{a}} \cos\left(\frac{\theta_3}{2}\right) = K_{\rho} \mathrm{d}r_1 \tag{12}$$

Also, from the moment equilibrium

$$f_{\mathrm{p}} \cos\left(\frac{\alpha}{2}\right)\left(\frac{r_1}{2}\right) = C_{\theta} \mathrm{d}\theta_3 + C_{\theta} \mathrm{d}\theta_2 \cos(\Psi) \tag{13}$$

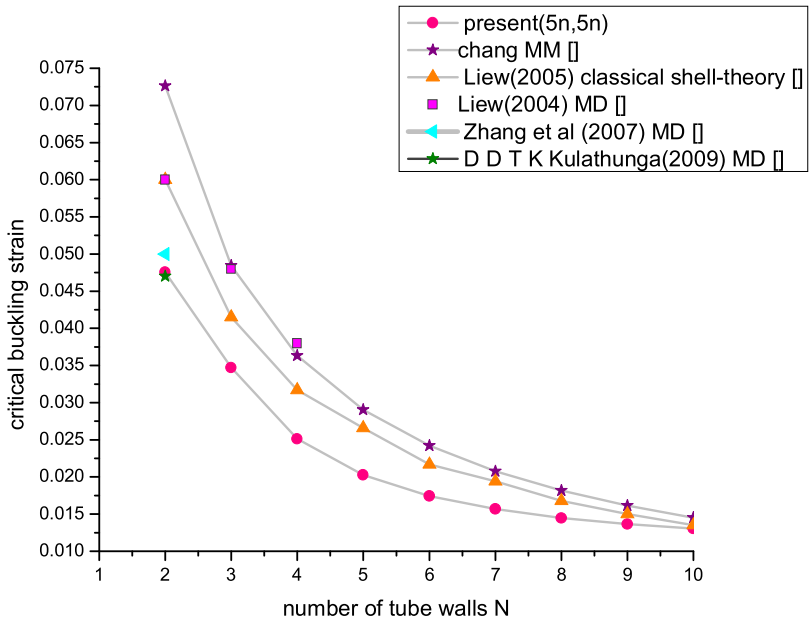

Fig. 9. Critical buckling strain as a function of number of tube walls N for different (5*n*,5*n*) armchair multiwalled carbon nanotubes.

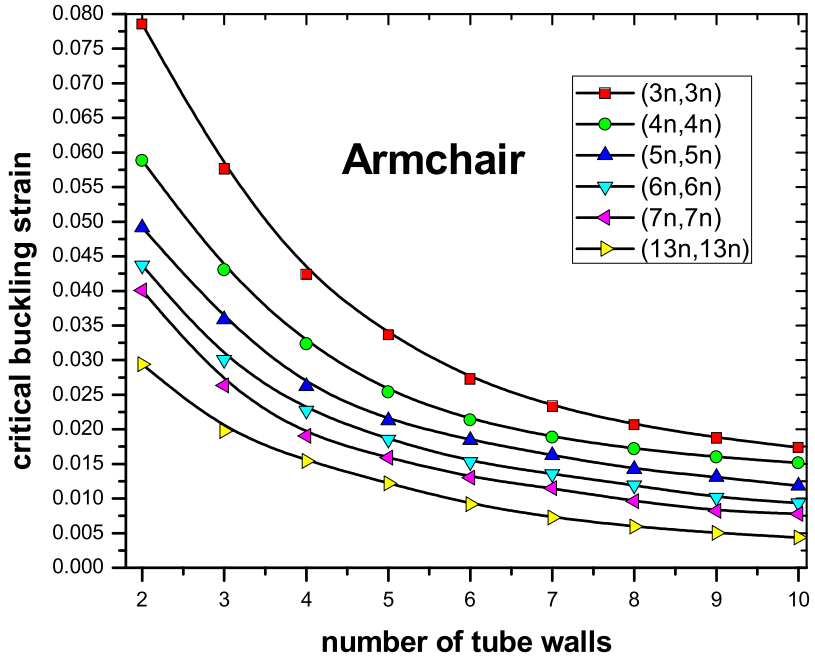

Fig. 10. Critical buckling strain as a function of number of tube walls N for different (*n*,*n*) armchair multiwalled carbon nanotubes.

where $C_\theta d\theta_3$ is the rotation moment induced by bond angle variation in plane $r_1 - r_2$, and $C_\theta d\theta_3\theta_2 \cos(\psi)$ the moment by $d\theta_3$ in plane $r_3 - r_1$. Ψ, the torsion angle between planes $r_1 - r_2$ and $r_3 - r_1$, can be calculated in [34]

$$\cos(\Psi) = \frac{\tan(\theta_3/2)}{\tan(\theta_2)} \tag{14}$$

The geometrical relationship between angles θ_3 and θ_2 is also given by

$$\cos(\theta_2) = -\cos\left(\frac{\pi}{n+m}\right)\cos\left(\frac{\theta_3}{2}\right) \tag{15}$$

where $\pi/(n+m)$ is the angle of bond r_3 to the plane $r_1 - r_2$. By differentiating both sides of Eq. (15), one can arrive at

$$d\theta_2 = -\frac{d\theta_3\left(\sin(\theta_3/2)\cos(\pi/(n+m))\right)}{2\sin(\theta_2)} \tag{16}$$

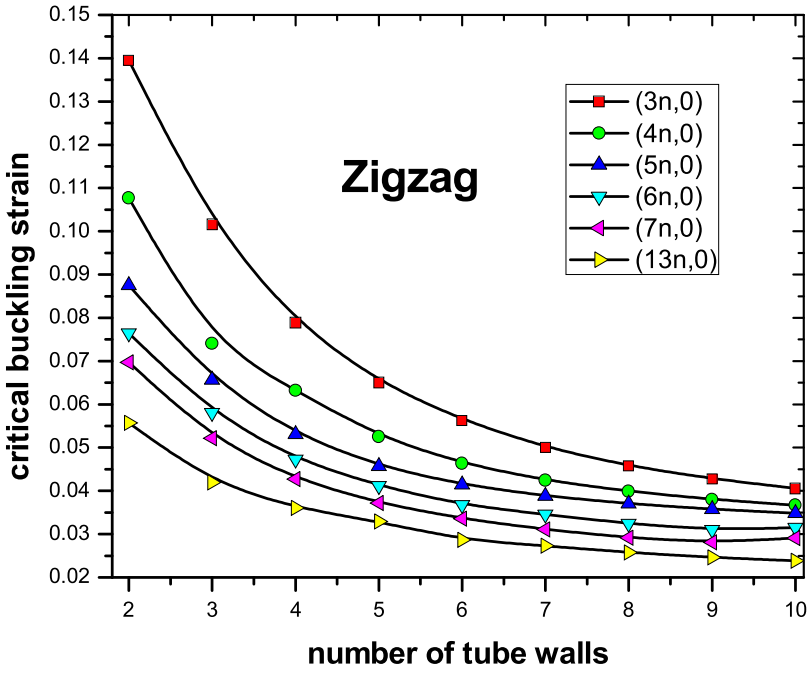

Fig. 11. Critical buckling strain as a function of number of tube walls N for different (*n*,0) zigzag multiwalled carbon nanotubes.

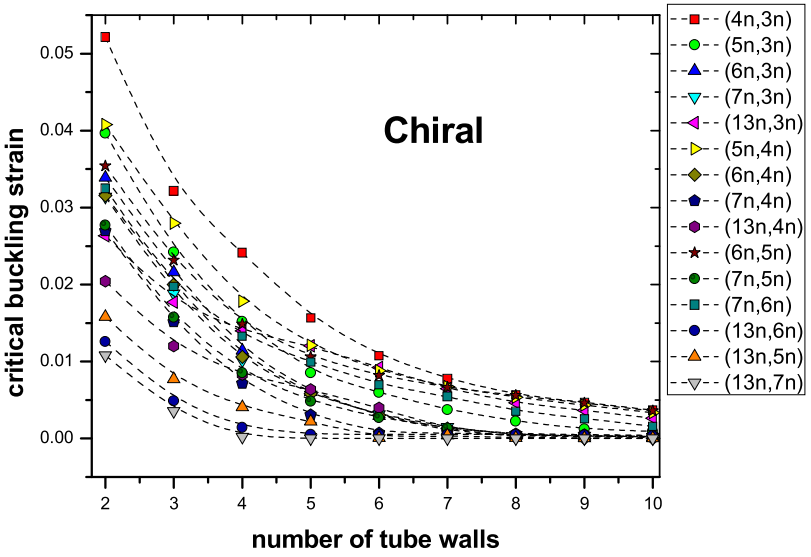

Fig. 12. Critical buckling strain as a function of number of tube walls N for different (*n*,*m*) chiral multiwalled carbon nanotubes.

Substituting Eqs. (14) and (16) into Eq. (13) with the assumption of $r_3 = r_1$ for the undeformed chiral single-walled CNT, the relation between $d\theta_3$ and dr_1 becomes

$$d\theta_3 = \frac{dr_1}{r_1}\frac{\cot\left(\theta_3/2\right)\left(2\lambda_A K_\rho r_1^2\right)}{C_\theta} \tag{17}$$

in which

$$\lambda_A = \frac{\sin\left(\theta_2 \cot\theta_3/2\right)}{\left(4\sin\left(\theta_2\right)\cot\left(\theta_3/2\right) - 2\sin\left(\theta_3/2\right)\cot\left(\theta_2\right)\cos\left(\pi/(n+m)\right)\right)}$$

The axial strain ϵ_{f^p} and circumferential strain $\epsilon_f^{'p}$ of a (*n*,*m*) chiral nanotube can be defined as [34],

$$\epsilon_{f^p} = \frac{d\left[r_1\sin\left(\theta_3/2\right) + r_2\sin\left(\theta_3/2\right)\right]}{r_1\sin\left(\theta_3/2\right) + r_2\sin\left(\theta_3/2\right)} \tag{19}$$

$$\epsilon_f^{'p} = \frac{d\left[r_3 + r_1\cos\left(\theta_3/2\right)\right]}{r_3 + \cos\left(\theta_3/2\right)} \tag{20}$$

By means of Eqs. (12)–(14), (16), (19), and (20), with the simplified relation $r_3 = r_1$, one has

$$\epsilon_f{}^p = \frac{dr_1}{r_1}\left(\frac{\cot\left(\theta_3/2\right)^2 \lambda_A K_\rho r_1^2}{C_\theta} + 1\right) \tag{21}$$

$$\epsilon_f^{'p} = \frac{dr_1}{r_1}\frac{\cos\left(\theta_3/2\right)}{1+\cos\left(\theta_3/2\right)}\left(1 - \frac{\lambda_A K_\rho r_1^2}{C_\theta}\right) \tag{22}$$

In accordance with its definition, the Young's modulus and Poisson's ratio of a chiral SWCNT can be written as [34]

$$Y_f^p = \frac{f_p}{2\pi R t \varepsilon_f{}^p} \tag{23}$$

$$\upsilon = -\frac{\varepsilon_1}{\varepsilon_0} \tag{24}$$

After a lengthy manipulation, Young's modulus and Poisson's ratio of chiral SWCNT can be given as follows

$$Y = \frac{1}{2\pi R t}\left(\frac{(n+m)k_\rho r_1}{\sin\left(\frac{\pi}{3}+\Theta\right)\sin\left(\frac{\theta_3}{2}\right)\left(\frac{\lambda_A K_\rho r_1^2}{C_\theta \tan\left(\frac{\theta_3}{2}\right)^2}+1\right)}\right) \tag{25}$$

$$\upsilon = -\frac{\cos\left(\theta_3/2\right)\left(1-\frac{\lambda_A K_\rho r_1^2}{C_\theta}\right)}{\left(1+\cos\left(\theta_3/2\right)\right)\left(\frac{\lambda_A K_\rho r_1^2}{C_\theta \tan\left(\frac{\theta_3}{2}\right)^2}+1\right)} \tag{26}$$

where, the thickness of a SWCNT, has many various values given by different people [35–37], and evidently, this situation can bring out great chaos. So, in the present study, the concept of surface Young's modulus would be introduced to avoid defining the magnitude of effective thickness. The so-called surface Young's modulus, then, can be expressed as the product of the conventional Young's modulus with the tube thickness, that is, $Y_s = Yt$

$$Y_S = \frac{1}{2\pi R}\left(\frac{(n+m)k_\rho r_1}{\sin\left(\pi/3+\Theta\right)\sin\left(\theta_3/2\right)\left(\frac{\lambda_A K_\rho r_1^2}{C_\theta \tan\left(\theta_3/2\right)^2}+1\right)}\right. \tag{27}$$

Using Eq. (21), one would have

$$dr_{ij1} = \left(\frac{\varepsilon_f{}^p r_1}{\left(\cot\left(\theta_3/2\right)^2 \lambda_A K_\rho r_1^2\right)/C_\theta + 1}\right) \tag{28}$$

dr_{ij2} is also obtained as same as above approach:

$$dr_{ij2} = \left(\frac{\varepsilon_f{}^p r_2}{\left(\frac{\cot\left(\theta_3/2\right)^2 \lambda_A K_\rho r_2^2}{C_\theta}+1\right)}\right) \tag{29}$$

dr_{ij3} is obtained By means of Eqs. (12)–(14), (16) and (19)

$$dr_{ij3} = \left(\frac{\tan\left(\frac{\pi}{6}-\Theta\right)}{K_\rho}\right)\left(C_\theta d\theta_3 + C_\theta d\theta_1 \frac{\tan\left(\theta_3/2\right)}{\tan\left(\theta_2\right)}\right)\left(\frac{1}{\cos\left(\theta_3/2\right)\left(r_3/2\right)}\right) \tag{30}$$

$$d\theta_{ij1} = -\frac{d\theta_{ij3}\sin\left(\theta_3/2\right)\cos\left(\pi/(n+m)\right)}{2\sin\left(\theta_2\right)} \tag{31}$$

$$d\theta_{ij2} = -\frac{d\theta_{ij3}\sin\left(\theta_3/2\right)\cos\left(\pi/(n+m)\right)}{2\sin\left(\theta_2\right)} \tag{32}$$

$$d\theta_{ij3} = \frac{dr_{ij1}}{r_1}\frac{\cot(\theta_3/2)\left(2\lambda_A K_\rho r_1^2\right)}{C_\theta} \tag{33}$$

According to the displacement of the atoms of SWCNT after buckling, the variations of bond length (Δr_{ij1}, Δr_{ij2}, Δr_{ij3}), bond angle ($\Delta\theta_{ij1}$, $\Delta\theta_{ij2}$, $\Delta\theta_{ij3}$), and inversion angle ($\Delta\beta_{ij}$) of the deformed SWCNT after buckling can be obtained. These quantities are given in the Appendix A in which the following parameters are used

$$\alpha_1 = 0 \tag{34-a}$$

$$\alpha_2 = \arcsin\left(\frac{r_3}{2R}\sin\left(\pi/3+\Theta\right)\right) \tag{34-b}$$

$$\alpha_3 = \arcsin\left(\frac{r_1}{2R}\sin\left(-\theta_3/2+\frac{\pi}{3}+\Theta\right)\right) \tag{34-c}$$

$$\alpha_4 = \arcsin\left(\frac{r_2}{2R}\sin\left(\theta_3/2+\frac{\pi}{3}+\Theta\right)\right) \tag{34-d}$$

where R, the tube radius can be expressed in the form

$$R = \frac{r_0\sqrt{3\left(n^2+nm+m^2\right)}}{2\pi} \tag{35}$$

where $\xi_{i,j}$, the radial displacement of the atom ij, is assumed to be small in comparison with r_0 For atoms located at type B position as shown in Fig. 2, the term$\xi_{i,j+1}$ in the preceding equations must be replaced by $\xi_{i,j-1}$. In fact, there is no crucial difference between atoms at type A and type B positions. For convenience, the mathematical procedure described herein is only for atoms at a type A position.

2.3. Calculation of force constants

2.3.1. Mechanical properties of graphene using density functional theory (DFT)

Due to superficial properties of two-dimensional monolayer honeycomb structures of graphene, they can be implemented for the future applications. Through extraordinary mechanical properties of honeycomb structure of graphene with sp^2 bonding, they have the capability to offer high in-plane strength. Carbon nanotubes which are formed by rolling up the graphene sheets provide the highest tensile strength and elastic modulus compared to any other known materia. In this section, the elastic constants of graphene based on the strain energy calculations are presented in the range of harmonic deformation. The calculations are performed on the basis of density functional theory (DFT), in the form of generalized gradient approximation (GGA) and using exchange correlation of Perdew–Burke–Ernzerhof (PBE). The calculations presented herein are performed via the Quantum–Espresso coding procedure. The basic concepts and relations used in the Quantum–Espresso code are expressed as follows.

2.3.1.1. Calculating band structure. A group of atoms which contains many numbers of electrons and ions is considered. In this collection, there are interactions between the ions and electrons which cause to create an electronic structure. These interactions can be expressed accurately using the Schrodinger many body equation as

$$H\Psi\left((r_1, r_2, \ldots, r_N); \{R_m\}\right) = E\Psi\left((r_1, r_2, \ldots, r_N); \{R_m\}\right) \tag{36}$$

where r_i is the location of ith electron, and R_m is equal to the location of the ions which based on the Born–Oppenheimer, approximation can be regard constant. The related Hamiltonian operator can be defined as follows

$$H = \frac{-1}{2}\sum_i \nabla_i^2 + \sum_{i<j}\frac{1}{|r_i - r_i|} + \sum_i V_{ext}\left(r_i, \{R_m\}\right) \tag{37}$$

which includes the expressions of kinetic energy, interactions of electron–electron, and potential energy, respectively. Through minimizing the total energy with respect to R_m, the equilibrium location of the ions can be obtained. By solving the above equation corresponding to all particles, a complete data of the system will be available. However, it is not possible to solve these 3N equations for a system with high numbers of atoms. So, to find a solution for this problem, the density functional theory (DFT) is utilized which can be defined as

$$n(r) = N\int dr_2 \ldots \int dr_N |\Psi\left((r_1, r_2, \ldots, r_N); \{R_m\}\right)|^2 \tag{38}$$

On the basis of DFT and using Hohenberg–Kohn equations, all of the properties of a molecular system can be calculated.

2.3.1.2. Kohn–Sham equations. the following set of one-particle equations as recessive relations to obtain the energy of the ground state and density of the electrons in this state can be expressed as

$$\left[\frac{-1}{2}\nabla^2 + V_{eff}(r)\right]\Psi_i(r) = \varepsilon_i\Psi_i(r) \tag{39},$$

$$V_{eff}(r) = V_H(r) + V_{xc}(r) + V_{ext}(r) \quad ,$$

$$n(r) = \sum_{i=1}^{N}|\Psi_i(r)|^2$$

$$V_H(r) = \int \frac{n(r)}{|r - r'|}dr' \quad ,$$

$$V_{xc}(r) = \frac{\partial E_{xc}[n(r)]}{\partial n(r)}$$

In the present formulation, the complex interaction of electron to electron is represented by the Hartree potential and exchange correlation term.

2.3.1.3. Local density approximation (LDA). The recessive solution of Kohn–Shem is an efficient procedure for the solid state physical problems. Nonetheless, to use this strong method, it is necessary to estimate the exchange-correlation functional which is not actually available. So, to evaluate this function, a new approximation should be employed that in the current study, the simplest one which is known as local density approximation is utilized. According to this type of approximation, the exchange-correlational energy relevant to an electron in a homogenous electronic gas is deducted for an inconsistent distribution as follows

$$E_{xc}^{LDA}[n(r)] = \int n(r)\,\varepsilon_{xc}^{n_0}[n(r)]\,dr \tag{40}$$

2.3.1.4. Pseudopotential approximation. Internal electrons in atoms do not have a considerable effect on the electron–electron interactions. Therefore, only the valence electrons are included in the Kohn–Shem equations. Though this matter make increase the computational efficiency of the solution, but wave functions of valence electrons change rapidly in the cores of the atoms which causes difficulty to solve the problem numerically. To overcome this difficulty, the potentials of the ions and inner electrons are replaced with plane potential named as Pseudopotential. Based on the previous works in the literature, the change in the results is not significant with increasing the unit cell dimension. Therefore, in the current study, the smallest hexagonal unit cell is utilized in the calculations for more simplicity. Brillouin zone integration is conducted with 20* 20* 1 Monkhorst and Pack k-point mesh, and the cut-off energy for plane wave expansion was taken to be 80*Ry*. The graphene has a 2D hexagonal unit cell with a lattice constant of $a = 2046$ Å in which the C—C bond length is $d = 1042$ Å and all atoms lie in the same plane.

2.3.2. Young's modulus and Poisson's ratio

The two essential constants to represent the elastic properties of a homogenous and isotropic material are Young's modulus and Poisson's ratio. Due to inconsistency for the value of effective thickness of monolayer structures, it is better to use the in-plane stiffness in spite of young's modulus.

If A_0 is the equilibrium area of the system, the in-plane stiffness can be calculated as

$$Y_s = \left(\frac{1}{A_0}\right) \times \left(\frac{\partial {E_S}^2}{\partial \varepsilon^2}\right) \tag{41}$$

in which E_s is the strain energy given by

$$E_s = E_T(\varepsilon) - E_T(\varepsilon = 0) \tag{42}$$

which is equal to the total energy at a given axial strain ε minus the total energy at zero strain. And ε is the uniaxial strain ($\varepsilon = \frac{\Delta a}{a}$, abeing the lattice constant). The Poisson's ratio which is defined as the ratio of the transverse strain to the axial strain can be expressed as

$$\nu = \frac{-\varepsilon_{trans}}{\varepsilon_{axial}} \tag{43}$$

Fig. 4 which shows the harmonic region can be taken between $-0.02 < \varepsilon < 0.02$ and it is followed by an inharmonic region where higher order terms are not negligible in the strain energy equation. The calculated value of Y_s in the harmonic region is equal to 350 N/m for graphene. Also the obtained Poisson's ratio is 0.16. The value of in-plane stiffness obtained in this work relevant to graphene has a good agreement with the experimental value of 340 ± 50N/m which confirms the reliability of the present method. Fig. 5 depicts the variation of strain energy ES and its derivative $\left[dE_S(\varepsilon)/d\epsilon\right]$ with the applied strain varying from −0.02 to 0.45 in uniform expansion. It is observed from the figure that there are two critical values of strain. The first one, ε_{C_1}, is the point corresponding to which the derivative curve reaches to its maximum value and then tends to be decreased. It occurs nearly at $\varepsilon = 0.19$. It means that for $\varepsilon > \varepsilon_{C_1}$, the expansion of structure can be happened with smaller tensions. After the inharmonic region, a plastic region can be found where irreversible structural changes occur in the system corresponding to which the structure behave in a different manner after the yielding point. The second critical point ε_{C_2} is the yielding point which is approximately equal to $\varepsilon = 0.28$. For the strains with the values higher than this point, the strain energy tends to be increased and the system remains its honeycomblike type of the structure. Because of the release of tension, all the deformation become extinct, so the system could return to its initial size at $\varepsilon = 0$. Apparently, for a perfect graphane subjected to uniform strain of ε_{C_2}, the yielding can only occur for ideal conditions. For $\varepsilon_{C_1} < \varepsilon < \varepsilon_{C_2}$ the system is in a metastable state. Following the yielding point, where $\varepsilon \geq \varepsilon_{C_2}$, the irreversible deformations will be found corresponding to the plastic range. However, this range of strain is beyond the scope of this paper.

2.3.3. Flexural rigidity

Flexural rigidity is an important property of a two dimensional sheet of material, i.e., the dependence of the strain energy on its curvature along some direction. By bending of a grapheme sheet, one can obtain SWCNT's of different chirality. We can define the value of flexural rigidity D as a coefficient in energy of unloaded/free relaxed tube as a function of its diameter

$$D = \frac{\partial^2 E}{\partial K^2} \tag{44}$$

where $K(1/R)$ is the only nonvanishing principal curvature of the monolayer.

Tube energy per atom relative to a flat graphene sheet is the same as the graphene sheet strain energy due to flexing. Fig. 6 represents the strain energy relative to planar graphene for fully relaxed nanotubes of varying radius vs a quadratic approximation of the bending energy with the flexural modulus predicted by the Density functional theory (DFT) theory. The value of the flexural modulus D determined from larger diameter CNTs is 0.8586 eV (2.249 eV Å^2/atom), and is independent of whether (n,n) or $(n,0)$ structures are considered. And indeed, our results for fully optimized tubes do confirm that there is no difference in strain energy for (n,n) and $(n,0)$ carbon, Which shows that there is no difference in values of the flexural rigidity D for tubes of varying chirality, it means these materials are isotropic. This number is in good agreement with the molecular dynamics (MD) simulations based values of 0.85 eV computed by Yakobson [19].

2.3.4. Force constants K_ρ, C_θ *and* C_ω

Substituting $\theta_3 = \theta_2 = 2\pi/3$ and n$\sim\infty$ into Eqs. (26) and (27) give the expressions for the elastic modulus and Poisson's ratio in the plane of graphene as follows,

$$Y_S = \frac{8\sqrt{3}K_\rho}{K_\rho r_1^2/C_\theta + 18} \tag{45}$$

$$\upsilon = \frac{K_\rho r_1^2/C_\theta - 6}{K_\rho r_1^2/C_\theta + 18} \tag{46}$$

By introducing the computed values of elastic modulus, Poisson's ratio and flexural rigidity D, which are equal to $350N/m$, 0.16 and 0.8586 eV respectively, into the preceding equations, one can obtain $K_\rho = 721.69nN/n$ and $C_\theta = 1.376nNnm$. Also the value of C_ω can be calculated as $24D$ [19], which will lead to $C_\omega = 3.30nNnm$.

In this paper, similar to Ru's multishell model, we only consider the van der Waals interactions from the nearest neighboring layers and simply take $K_{vdw} = K_v = 1.62$nN/nm, which is in fact the value for an atom interacting with a graphene sheet to which the distance from the atom is about 0.34 nm.

2.4. Stability equation

Making use of the parameters disscussed in Section 2.2, the potential energy of the system prior to buckling, dE, and after buckling, ΔE, can be computed using Eq. (19). The free energy of the system, Π, is

$$\Pi = \mathrm{dE} - \Delta E \tag{47}$$

The condition for Π to be extremum requires

$$\frac{\partial \Pi}{\partial \xi_{ij}} = \frac{\partial(\mathrm{dE} - \Delta E)}{\partial \xi_{ij}} = 0 \tag{48}$$

where ij is the radial displacement of the atom ij.

Where the buckling mode parameter ξ for an (n, n) armchair nanotube can be expressed as

$$\xi = \frac{\sqrt{3}m_1\pi r_0}{2L} \tag{51}$$

here L is the tube length, r_0 the reference C—C bond length, and m_1 the number of half waves in the axial direction. It is seen that the buckling strain has a minimum value (i.e., the critical buckling strain) that decreases with increasing n (increasing tube diameter). With the aid of the buckling wavelength

$$l = \frac{\sqrt{3}\pi r_0}{\xi} \tag{52}$$

where ξ is defined in Eq. (40).

we can also see that the wavelength of the buckling increases with an increase in n [17]. Fig. 7 shows the variation of critical buckling strain versus carbon nanotube diameter for the state of armchair.

Also obtained results from Chang's molecular mechanic and Yakobson's [8] (or by Ru's [9]) continuum method are presented in Fig. 7 which shows large difference with those of molecular dynamic results.

To investigate the influence of the chirality on the buckling strains of nanotubes, the variation of critical buckling strain versus diameter of nanotube is plotted in Fig. 8 for armchair, zigzag and chiral tubes. The difference between results obtained for armchair and zigzag tubes becomes more pronounced when the diameter of tube increases. As it can be seen in this figure, the stability of zigzag carbon nanotube under axial load is better than armchair carbon nanotube and the minimum stability is for $(n, n/2)$ tube.

3. Buckling of MWCNT's under axial compression

For an k-walled CNT, although a diamond like mode can be observed at the final buckling stage, MD simulations have shown that the initial buckling mode of an MWCNT is in a ring pattern [30]. Thus the above approach is particular useful to determine the critical buckling strain of MWCNT's. The system free energy for an MWCNT is the summation of the intratube energies, $\mathrm{dE}_{\mathrm{intra}} - \Delta E_{\mathrm{intra}}$, and the intertube van der Waals interactions, $dE_{inter} - \Delta E_{inter}$,

$$\Pi = (dE_{\mathrm{intra}} - \Delta E_{\mathrm{intra}}) + (dE_{\mathrm{inter}} - \Delta E_{\mathrm{inter}}) = \sum_{K=1}^{N}\left(dE^{(K)} - \Delta E^{(K)}\right) + \sum_{K=1}^{N-1}\left(dE_{\mathrm{vdw}}^{(K,K+1)} - \Delta E_{\mathrm{vdw}}^{(K,K+1)}\right) \tag{53}$$

where the superscript k is the wall index numbered from the outermost tube to the innermost tube, $dE^{(K)}$ and $\Delta E^{(K)}$ are the intratube strain energies for the kth wall of the MWCNT, and $dE_{vdw}^{(K,K+1)}$ and $\Delta E_{vdw}^{(K,K+1)}$ represent the intertube van der Waals interaction potentials between the kth and $(k+1)$th individual tubes.

We seek the radial displacement of atom ij located on the kth wall due to axisymmetric buckling as

$$\xi_{ij} = \xi^{(k)}\left(x_{ij}\right) = Z^{(K)}\cos\left(\frac{m\pi x_{ij}}{L}\right) + Z_0^{(K)} \tag{54}$$

where L is the length of nanotube, m the half wave numbers along the tube axis direction, x_{ij} the longitudinal coordinate of atom ij, and $Z^{(K)}$ the bucking amplitude and $Z_0^{(K)}$ the radial extension of the nanotube before buckling. The extremum condition of Π leads to

$$\frac{\partial\Pi}{\partial\xi_{ij}} = \frac{\partial\left(dE^{(K)} - \Delta E^{(K)}\right)}{\partial\xi_{ij}} + \frac{K_{vdw}}{2}\frac{\partial}{\partial\xi_{ij}}\left\{\left[\xi^{(K+1)}\left(x_{ij}\right) - \xi^{(K)}\left(x_{ij}\right)\right]^2 + \left[\xi^{(K)}\left(x_{ij}\right) - \xi^{(K-1)}\left(x_{ij}\right)\right]^2\right\} = 0 \tag{55}$$

Here we should note that for an N-walled nanotube, $\xi^{(N+1)}(x) = \xi^{(0)}(x) = 0$. Eq. (55) in fact gives the radial equilibrium equation of atom i. When the van der Waals interaction is absent, Eq. (55) can be simplified to Eq. (48) for a SWNT. With use of Eq. (54) to keep Eq. (55) a permanent equation, it needs two constraint equations. One of them may be used to calculate $z_0^{(k)}$ and will not be discussed here because it has no contributions to the problem we considered. The other for $z^{(k)}$ can be written as

$$\left(F(\varepsilon_0)^{(K)}\right)Z^{(K)} - K_v\left(Z^{(K+1)} - 2Z^{(K)} + Z^{(K-1)}\right) = 0 \tag{56}$$

with $Z^{(N+1)} = Z^{(0)} = 0$ for an N-walled nanotube. Comparing Eq. (56)–(49), as can be expected, the characteristic equations for a MWNT are coupled by the intertube van der Waals interactions.

We rewrite Eq. (56) in a matrix form as

$$[M]\left\{Z\right\} = 0 \tag{57}$$

where the coefficient matrix

$$[M] = \begin{bmatrix} F(\varepsilon_0)^{(1)} + K_v & -K_v & 0 & \dots & 0 & 0 \\ -K_v & F(\varepsilon_0)^{(2)} + 2K_v & -K_v & \dots & 0 & 0 \\ 0 & -K_v & F(\varepsilon_0)^{(3)} + 2K_v & \dots & 0 & 0 \\ \dots & \dots & \dots & \dots & \dots & \dots \\ 0 & 0 & 0 & \dots & F(\varepsilon_0)^{(N-1)} + 2K_v & -K_v \\ 0 & 0 & 0 & \dots & -K_v & F(\varepsilon_0)^{(N)} + K_v \end{bmatrix} \tag{58}$$

and the vector **z** represents the buckling amplitude of each individual tube:

$$\{z\} = \left\{z^{(1)}, z^{(2)}z^{(3)}, \dots, z^{(N)}\right\}^T \tag{59}$$

Nontrivial solution of **z** need the determinant of matrix M to be zero—i.e.,

$$\mathrm{Det}\,[M] = 0 \tag{60}$$

which consequently yields an k-order equation of ε_0. The buckling strain ε_0 corresponding to a given buckling mode for any k-walled tubes, in principle, can be obtained from such an k-order equation, and the critical buckling strain ε_C should be the minimum value of ε_0.

The critical buckling load of an MWNT under axial compression can be determined from Eq. (60). For any given buckling mode parameter ξ, there exist N solutions of Eq. (60). With the variation of ξ from 0 to $\pi/2$, there is a minimum value among these solutions which is the critical buckling strain of the problem.

4. Results and discussion

The critical buckling strain of $(5n,5n)$ MWNT's (which can be viewed as solid MWCNT when $k>2$) is shown in Fig. 9. We can see that the critical buckling strain decreases with increasing layers of the MWCNT (i.e., increasing outer diameter of the MWNT) under both load conditions. This phenomenon is quite different from that of a continuum shell due to the fact that the intertube van der Waals interaction is much weaker than the intratube binding interaction, which makes the MWCNT's highly anisotropic.

As it can be found from Fig. 9, the difference between critical axial buckling strain of MWCNTs with various numbers of tubes is more siginificant corresponding to lower numbers of tubes and by increasing of k, this difference tends to diminished. This obtained pattern is in good agreement with the results reported in the literature using MD simulations.

After the validation of the present solution, now the results for the general chiral nanotubes can be given. Illustrated in Figs. 10–12 are the variation of critical axial buckling strain of armchair, zigzag, and chiral MWCNTs with the number of tube walls, respectively. As it can be observed from the figure, the variation of critical axial buckling strain of MWCNTs in general form will be decreaseed by increasing the number of tube walls and this decrease is more considerable relevant to lower values of chiral number n.

Appendix A.

Stretching of bond r_1 after buckling:

$$\Delta r_{ij1} = \frac{1}{2r_1}(\xi_{i-1,j}^2 + \xi_{i,j}^2 - 2\xi_{i-1,j}\cos(\alpha_3)\xi_{i,j}\cos(\alpha_1) - 2\xi_{i-1,j}\sin(\alpha_3)\xi_{i,j}\sin(\alpha_1) + \cos\left(\frac{\theta_3}{2}\right)\sin\left(\Theta\right)\xi_{i-1,j}\sin(\alpha_3)r_1$$
$$- \cos\left(\frac{\theta_3}{2}\right)\sin\left(\Theta\right)\xi_{i,j}\sin(\alpha_1)r_1 + \sqrt{3}\sin\left(\frac{\theta_3}{2}\right)\sin\left(\Theta\right)\xi_{i-1,j}\sin(\alpha_3)r_1 - \sin\left(\frac{\theta_3}{2}\right)\cos\left(\Theta\right)\xi_{i-1,j}\sin(\alpha_3)r_1$$
$$+ \sin\left(\frac{\theta_3}{2}\right)\cos\left(\Theta\right)\xi_{i,j}\sin(\alpha_1)r_1 - \sqrt{3}\sin\left(\frac{\theta_3}{2}\right)\sin\left(\Theta\right)\xi_{i,j}\sin(\alpha_1)r_1 + \sqrt{3}\cos\left(\frac{\theta_3}{2}\right)\cos\left(\Theta\right)\xi_{i-1,j}\sin(\alpha_3)r_1$$
$$- \sqrt{3}\cos\left(\frac{\theta_3}{2}\right)\cos\left(\Theta\right)\xi_{i,j}\sin(\alpha_1)r_1) + \mathrm{d}r_{ij1} \tag{1-A}$$

Stretching of bond r_2 after buckling:

$$\Delta r_{ij2} = \frac{1}{2r_2}(\xi_{i+1,j}^2 + \xi_{i,j}^2 - 2\xi_{i+1,j}\cos(\alpha_4)\xi_{i,j}\cos(\alpha_1) - 2\xi_{i+1,j}\sin(\alpha_4)\xi_{i,j}\sin(\alpha_1) + \cos\left(\frac{\theta_3}{2}\right)\sin\left(\Theta\right)\xi_{i+1,j}\sin(\alpha_4)r_2$$
$$- \cos\left(\frac{\theta_3}{2}\right)\sin\left(\Theta\right)\xi_{i,j}\sin(\alpha_1)r_2 + \sqrt{3}\sin\left(\frac{\theta_3}{2}\right)\sin\left(\Theta\right)\xi_{i+1,j}\sin(\alpha_4)r_2 - \sin\left(\frac{\theta_3}{2}\right)\cos\left(\Theta\right)\xi_{i+1,j}\sin(\alpha_4)r_2$$
$$+ \sin\left(\frac{\theta_3}{2}\right)\cos\left(\Theta\right)\xi_{i,j}\sin(\alpha_1)r_2 - \sqrt{3}\sin\left(\frac{\theta_3}{2}\right)\sin\left(\Theta\right)\xi_{i,j}\sin(\alpha_1)r_2 + \sqrt{3}\cos\left(\frac{\theta_3}{2}\right)\cos\left(\Theta\right)\xi_{i+1,j}\sin(\alpha_4)r_2$$
$$- \sqrt{3}\cos\left(\frac{\theta_3}{2}\right)\cos\left(\Theta\right)\xi_{i,j}\sin(\alpha_1)r_2) + \mathrm{d}r_{ij2} \tag{2-A}$$

Stretching of bond r_3 after buckling:

$$\Delta r_{ij3} = \frac{1}{2r_3}(\xi_{i,j+1}^2 + \xi_{i,j}^2 - 2\xi_{i,j+1}\cos(\alpha_2)\xi_{i,j}\cos(\alpha_1) + 2\xi_{i,j+1}\sin(\alpha_2)\xi_{i,j}\sin(\alpha_1) + \sin\left(\Theta\right)\xi_{i,j+1}\sin(\alpha_2)r_3 + \sin\left(\Theta\right)\xi_{i,j}\sin(\alpha_1)r_3$$
$$+ \sqrt{3}\cos\left(\Theta\right)\xi_{i,j+1}\sin(\alpha_2)r_3 + \sqrt{3}\cos\left(\Theta\right)\xi_{i,j}\sin(\alpha_1)r_3) \tag{3-A}$$

Variation of bond angle θ_1 after buckling:

$$\Delta\theta_{ij1} = -\left(\frac{1}{2\sqrt{3}(r_1r_2)^{\frac{1}{2}}}\right)((\frac{-1}{2\left(-1+\cos\left(\theta_1\right)^2\right)\sqrt{1-\cos\left(\theta_1\right)^2}}(2(\sin\left(\Theta\right)\xi_{i,j}\sin(\alpha_1)r_3 - 2\xi_{i+1,j}\sin(\alpha_4)\xi_{i,j}\sin(\alpha_1)$$
$$+ 2\xi_{i,j+1}\sin(\alpha_2)\xi_{i,j}\sin(\alpha_1) - 2\xi_{i,j+1}\cos(\alpha_2)\xi_{i,j}\cos(\alpha_1) - \sin\left(\frac{\theta_3}{2}\right)\cos\left(\Theta\right)\xi_{i,j}\sin(\alpha_1)r_2 + 2{\xi_{i,j}}^2$$
$$- \cos\left(\frac{\theta_3}{2}\right)\sin\left(\Theta\right)\xi_{i,j}\sin(\alpha_1)r_2 - 2r_2\cos\left(\frac{\theta_3}{2}\right)\sin\left(\Theta\right)^2r_3 - 2\xi_{i+1,j}\cos(\alpha_4)\xi_{i,j}\cos(\alpha_1) - 2r_2r_3\cos\left(\frac{\theta_3}{2}\right)\cos\left(\Theta\right)^2$$
$$- 2\xi_{i+1,j}\sin(\alpha_4)\xi_{i,j+1}\sin(\alpha_2) + \sqrt{3}\sin\left(\frac{\theta_3}{2}\right)\sin\left(\Theta\right)\xi_{i,j}\sin(\alpha_1)r_2 - \sqrt{3}\cos\left(\frac{\theta_3}{2}\right)\cos\left(\Theta\right)\sin(\alpha_1)\xi_{i,j}r_2$$
$$+\sqrt{3}\cos\left(\Theta\right)\xi_{i,j}\sin(\alpha_1)r_3 + \sqrt{3}\sin\left(\frac{\theta_3}{2}\right)\sin\left(\Theta\right)\xi_{i,j+1}\sin(\alpha_2)r_2 - \sin\left(\frac{\theta_3}{2}\right)\cos\left(\Theta\right)\xi_{i,j+1}\sin(\alpha_2)r_2$$
$$- \sqrt{3}\cos\left(\frac{\theta_3}{2}\right)\cos\left(\Theta\right)\xi_{i,j+1}\sin(\alpha_2)r_2 - \cos\left(\frac{\theta_3}{2}\right)\sin\left(\Theta\right)\xi_{i,j+1}\sin(\alpha_2)r_2 - \xi_{i+1,j}\sin(\alpha_4)r_3\sin\left(\Theta\right)$$
$$-\sqrt{3}\xi_{i+1,j}\sin(\alpha_4)r_3\cos\left(\Theta\right) + 2\xi_{i+1,j}\cos(\alpha_4)\xi_{i,j+1}\cos(\alpha_2))\cos\left(\theta_1\right)^3 - 3\cos\left(\theta_1\right)^2 - (\sin\left(\Theta\right)\xi_{i,j}\sin(\alpha_1)r_3$$
$$-2\xi_{i+1,j}\sin(\alpha_4)\xi_{i,j}\sin(\alpha_1) + 2\xi_{i,j+1}\sin(\alpha_2)\xi_{i,j}\sin(\alpha_1) - 2\xi_{i,j+1}\xi_{i,j}\cos(\alpha_2)\cos(\alpha_1) - \sin\left(\frac{\theta_3}{2}\right)\xi_{i,j}\cos\left(\Theta\right)\sin(\alpha_1)r_2 + 2{\xi_{i,j}}^2$$
$$- \cos\left(\frac{\theta_3}{2}\right)\sin\left(\Theta\right)\xi_{i,j}\sin(\alpha_1)r_2 - 2r_2r_3\cos\left(\frac{\theta_3}{2}\right)\sin\left(\Theta\right)^2 + 2{\xi_{i,j}}^2 - 2\xi_{i+1,j}\cos(\alpha_4)\xi_{i,j}\cos(\alpha_1) - 2r_2r_3\cos\left(\frac{\theta_3}{2}\right)\cos\left(\Theta\right)^2$$
$$-2\xi_{i+1,j}\sin(\alpha_4)\xi_{i,j+1}\sin(\alpha_2) + \sqrt{3}\sin\left(\frac{\theta_3}{2}\right)\sin\left(\Theta\right)\xi_{i,j}r_2\sin(\alpha_1) - \sqrt{3}\cos\left(\frac{\theta_3}{2}\right)\cos\left(\Theta\right)\xi_{i,j}\sin(\alpha_1)r_2$$

$$+\sqrt{3}\cos\left(\Theta\right)\xi_{i,j}\sin\left(\alpha_1\right)r_3+\sqrt{3}\sin\left(\frac{\theta_3}{2}\right)\sin\left(\Theta\right)\xi_{i,j+1}r_2\sin\left(\alpha_2\right)-\sin\left(\frac{\theta_3}{2}\right)\cos\left(\Theta\right)\xi_{i,j+1}\sin\left(\alpha_2\right)r_2$$

$$-\sqrt{3}\cos\left(\frac{\theta_3}{2}\right)\cos\left(\Theta\right)\xi_{i,j+1}\sin\left(\alpha_2\right)r_2-r_2\cos\left(\frac{\theta_3}{2}\right)\sin\left(\Theta\right)\xi_{i,j+1}\sin\left(\alpha_2\right)-\xi_{i+1,j}\sin\left(\alpha_4\right)r_3\sin\left(\Theta\right)$$

$$-\sqrt{3}\xi_{i+1,j}\sin\left(\alpha_4\right)r_3\cos\left(\Theta\right)+2\xi_{i+1,j}\cos\left(\alpha_4\right)\xi_{i,j+1}\cos\left(\alpha_2\right))^2+2))\left(\cos\left(\theta_1\right)\right)-(\sin\left(\Theta\right)\xi_{i,j}\sin\left(\alpha_1\right)r_3-2\xi_{i+1,j}\sin\left(\alpha_4\right)\xi_{i,j}\sin\left(\alpha_1\right)$$

$$+2\xi_{i,j+1}\sin\left(\alpha_2\right)\xi_{i,j}\sin\left(\alpha_1\right)-2\xi_{i,j+1}\cos\left(\alpha_2\right)\xi_{i,j}\cos\left(\alpha_1\right)-\sin\left(\frac{\theta_3}{2}\right)\cos\left(\Theta\right)\xi_{i,j}\sin\left(\alpha_1\right)r_2-\cos\left(\frac{\theta_3}{2}\right)\sin\left(\Theta\right)\xi_{i,j}\sin\left(\alpha_1\right)r_2$$

$$-2r_2r_3\cos\left(\frac{\theta_3}{2}\right)+2{\xi_{i,j}}^2-2\xi_{i+1,j}\cos\left(\alpha_4\right)\xi_{i,j}\cos\left(\alpha_1\right)-2\xi_{i+1,j}\sin\left(\alpha_4\right)\xi_{i,j+1}\sin\left(\alpha_2\right)+\sqrt{3}\sin\left(\frac{\theta_3}{2}\right)\sin\left(\Theta\right)\xi_{i,j}\sin\left(\alpha_1\right)r_2$$

$$-\sqrt{3}\cos\left(\frac{\theta_3}{2}\right)\cos\left(\Theta\right)\xi_{i,j}\sin\left(\alpha_1\right)r_2+\sqrt{3}\cos\left(\Theta\right)\xi_{i,j}\sin\left(\alpha_1\right)r_3+\sqrt{3}r_2\sin\left(\frac{\theta_3}{2}\right)\sin\left(\Theta\right)\xi_{i,j+1}\sin\left(\alpha_2\right)$$

$$-r_2\sin\left(\frac{\theta_3}{2}\right)\cos\left(\Theta\right)\xi_{i,j+1}\sin\left(\alpha_2\right)-\sqrt{3}\cos\left(\frac{\theta_3}{2}\right)\cos\left(\Theta\right)r_2\xi_{i,j+1}\sin\left(\alpha_2\right)-r_2\cos\left(\frac{\theta_3}{2}\right)\sin\left(\Theta\right)\xi_{i,j+1}\sin\left(\alpha_2\right)$$

$$-\xi_{i+1,j}\sin\left(\alpha_4\right)r_3\sin\left(\Theta\right)-\sqrt{3}\xi_{i+1,j}\sin\left(\alpha_4\right)r_3\cos\left(\Theta\right)+2\xi_{i+1,j}\cos\left(\alpha_4\right)\xi_{i+1,j}\cos\left(\alpha_2\right))\left(\sin\left(\theta_1\right)\right))+\mathrm{d}\theta_{ij1} \tag{4-A}$$

Variation of bond angle θ_2. after buckling:

$$\Delta\theta_{ij2}=-\left(\frac{1}{2\sqrt{3}\left(r_1r_2\right)^{\frac{1}{2}}}\right)((\frac{-1}{2\left(-1+\cos\left(\theta_1\right)^2\right)\sqrt{1-\cos\left(\theta_1\right)^2}}(2(\sin\left(\Theta\right)\xi_{i,j}\sin\left(\alpha_1\right)r_3+2\xi_{i,j+1}\sin\left(\alpha_2\right)\xi_{i,j}\sin\left(\alpha_1\right)$$

$$-2\xi_{i-1,j}\sin\left(\alpha_3\right)\xi_{i,j}\sin\left(\alpha_1\right)-2\xi_{i,j+1}\cos\left(\alpha_2\right)\xi_{i,j}\cos\left(\alpha_1\right)-2\xi_{i-1,j}\cos\left(\alpha_3\right)\xi_{i,j}\cos\left(\alpha_1\right)-\sin\left(\Theta\right)\cos\left(\frac{\theta_3}{2}\right)\xi_{i,j}\sin\left(\alpha_1\right)r_1+2{\xi_{i,j}}^2$$

$$+\sqrt{3}\cos\left(\Theta\right)\xi_{i,j}\sin\left(\alpha_1\right)r_3+r_1\sin\left(\frac{\theta_3}{2}\right)\cos\left(\Theta\right)\xi_{i,j}\sin\left(\alpha_1\right)-\sqrt{3}r_1\xi_{i,j}\sin\left(\frac{\theta_3}{2}\right)\sin\left(\Theta\right)\sin\left(\alpha_1\right)$$

$$-\sqrt{3}r_1\cos\left(\frac{\theta_3}{2}\right)\cos\left(\Theta\right)\xi_{i,j}\sin\left(\alpha_1\right)-2r_1r_3\cos\left(\frac{\theta_3}{2}\right)\cos\left(\Theta\right)^2+2\xi_{i-1,j}\cos\left(\alpha_3\right)\xi_{i,j+1}\cos\left(\alpha_2\right)-2\xi_{i-1,j}\sin\left(\alpha_3\right)\xi_{i,j+1}\sin\left(\alpha_2\right)$$

$$-2r_1r_3\cos\left(\frac{\theta_3}{2}\right)\sin\left(\Theta\right)^2-\xi_{i-1,j}\sin\left(\alpha_3\right)r_3\sin\left(\Theta\right)-r_1\cos\left(\frac{\theta_3}{2}\right)\sin\left(\Theta\right)\xi_{i,j+1}\sin\left(\alpha_2\right)-\sqrt{3}\cos\left(\Theta\right)\xi_{i-1,j}\sin\left(\alpha_3\right)r_3$$

$$+r_1\sin\left(\frac{\theta_3}{2}\right)\cos\left(\Theta\right)\xi_{i,j+1}\sin\left(\alpha_2\right)-\sqrt{3}r_1\sin\left(\frac{\theta_3}{2}\right)\sin\left(\Theta\right)\xi_{i,j+1}\sin\left(\alpha_2\right)-\sqrt{3}r_1\cos\left(\frac{\theta_3}{2}\right)\cos\left(\Theta\right)\xi_{i,j+1}\sin\left(\alpha_2\right))\cos\left(\theta_2\right)^3$$

$$-3\cos\left(\theta_2\right)^2-(\sin\left(\Theta\right)\xi_{i,j}\sin\left(\alpha_1\right)r_3+2\xi_{i,j+1}\sin\left(\alpha_2\right)\xi_{i,j}\sin\left(\alpha_1\right)-2\xi_{i-1,j}\sin\left(\alpha_3\right)\xi_{i,j}\sin\left(\alpha_1\right)-2\xi_{i,j+1}\cos\left(\alpha_2\right)\xi_{i,j}\cos\left(\alpha_1\right)$$

$$-2\xi_{i-1,j}\cos\left(\alpha_3\right)\xi_{i,j}\cos\left(\alpha_1\right)-\cos\left(\frac{\theta_3}{2}\right)\sin\left(\Theta\right)\xi_{i,j}\sin\left(\alpha_1\right)r_1+2{\xi_{i,j}}^2+\sqrt{3}\cos\left(\Theta\right)\xi_{i,j}\sin\left(\alpha_1\right)r_3+\sin\left(\frac{\theta_3}{2}\right)\cos\left(\Theta\right)\xi_{i,j}\sin\left(\alpha_1\right)r_1$$

$$-\sqrt{3}\sin\left(\frac{\theta_3}{2}\right)\sin\left(\Theta\right)\xi_{i,j}\sin\left(\alpha_1\right)r_1-\sqrt{3}r_1\cos\left(\frac{\theta_3}{2}\right)\cos\left(\Theta\right)\xi_{i,j}\sin\left(\alpha_1\right)-2r_1r_3r_3\cos\left(\frac{\theta_3}{2}\right)\cos\left(\Theta\right)^2+2\xi_{i-1,j}\cos\left(\alpha_3\right)\xi_{i,j+1}\cos\left(\alpha_2\right)$$

$$-2\xi_{i-1,j}\sin\left(\alpha_3\right)\xi_{i,j+1}\sin\left(\alpha_2\right)-2r_1\cos\left(\frac{\theta_3}{2}\right)\sin\left(\Theta\right)^2r_3-\xi_{i-1,j}\sin\left(\alpha_3\right)r_3\sin\left(\Theta\right)-r_1\cos\left(\frac{\theta_3}{2}\right)\sin\left(\Theta\right)\xi_{i,j+1}\sin\left(\alpha_2\right)$$

$$-\sqrt{3}\xi_{i-1,j}\sin\left(\alpha_3\right)r_3\cos\left(\Theta\right)+\sin\left(\frac{\theta_3}{2}\right)\cos\left(\Theta\right)\xi_{i,j+1}\sin\left(\alpha_2\right)r_1-\sqrt{3}r_1\sin\left(\frac{\theta_3}{2}\right)\sin\left(\Theta\right)\xi_{i,j+1}\sin\left(\alpha_2\right)$$

$$-\sqrt{3}r_1\cos\left(\frac{\theta_3}{2}\right)\cos\left(\Theta\right)\xi_{i,j+1}\sin\left(\alpha_2\right))^2+2))\left(\cos\left(\theta_2\right)\right)-(\sin\left(\Theta\right)\xi_{i,j}\sin\left(\alpha_1\right)r_3+2\xi_{i,j+1}\sin\left(\alpha_2\right)\xi_{i,j}\sin\left(\alpha_1\right)-2\xi_{i-1,j}\sin\left(\alpha_3\right)\xi_{i,j}\sin\left(\alpha_1\right)$$

$$-2\xi_{i,j+1}\cos\left(\alpha_2\right)\xi_{i,j}\cos\left(\alpha_1\right)-2\xi_{i-1,j}\cos\left(\alpha_3\right)\xi_{i,j}\cos\left(\alpha_1\right)-\cos\left(\frac{\theta_3}{2}\right)\sin\left(\Theta\right)\xi_{i,j}\sin\left(\alpha_1\right)r_1+2{\xi_{i,j}}^2+\sqrt{3}\cos\left(\Theta\right)\xi_{i,j}\sin\left(\alpha_1\right)r_3$$

$$+\sin\left(\frac{\theta_3}{2}\right)\cos\left(\Theta\right)\xi_{i,j}\sin\left(\alpha_1\right)r_1-\sqrt{3}\sin\left(\frac{\theta_3}{2}\right)\sin\left(\Theta\right)\xi_{i,j}\sin\left(\alpha_1\right)r_1-\sqrt{3}\cos\left(\frac{\theta_3}{2}\right)\cos\left(\Theta\right)\xi_{i,j}\sin\left(\alpha_1\right)r_1$$

$$+2\xi_{i-1,j}\cos(\alpha_3)\xi_{i,j+1}\cos(\alpha_2)-2\xi_{i-1,j}\sin(\alpha_3)\xi_{i,j+1}\sin(\alpha_2)-2r_1r_3\cos\left(\frac{\theta_3}{2}\right)-r_3\xi_{i-1,j}\sin(\alpha_3)\sin\left(\Theta\right)$$

$$-r_1\cos\left(\frac{\theta_3}{2}\right)\sin\left(\Theta\right)\xi_{i,j+1}\sin(\alpha_2)-\sqrt{3}r_3\xi_{i-1,j}\sin(\alpha_3)\cos\left(\Theta\right)+r_1\sin\left(\frac{\theta_3}{2}\right)\cos\left(\Theta\right)\xi_{i,j+1}\sin(\alpha_2)$$

$$-\sqrt{3}r_1\sin\left(\frac{\theta_3}{2}\right)\sin\left(\Theta\right)\xi_{i,j+1}\sin(\alpha_2)-\sqrt{3}r_1\cos\left(\frac{\theta_3}{2}\right)\cos\left(\Theta\right)\xi_{i,j+1}\sin(\alpha_2))\left(\sin\left(\theta_2\right)\right))+\mathrm{d}\theta_{ij2} \tag{5-A}$$

Variation of bond angle θ_3 after buckling:

$$\Delta\theta_{ij3}=-\left(\frac{1}{2\sqrt{3}(r_1r_2)^{\frac{1}{2}}}\right)((\frac{-1}{2\left(-1+\cos\left(\theta_3\right)^2\right)\sqrt{1-\cos\left(\theta_3\right)^2}}(2(-2\xi_{i+1,j}\cos(\alpha_4)\xi_{i,j}\cos(\alpha_1)-2\xi_{i-1,j}\xi_{i,j}\sin(\alpha_3)\sin(\alpha_1)+2{\xi_{i,j}}^2$$

$$-\sqrt{3}\cos\left(\frac{\theta_3}{2}\right)\cos\left(\Theta\right)\xi_{i,j}\sin(\alpha_1)r_1-2\xi_{i-1,j}\cos(\alpha_3)\xi_{i,j}\cos(\alpha_1)-\sqrt{3}\sin\left(\frac{\theta_3}{2}\right)\sin\left(\Theta\right)\xi_{i-1,j}\sin(\alpha_3)r_2$$

$$+\sin\left(\frac{\theta_3}{2}\right)\cos\left(\Theta\right)\xi_{i-1,j}\sin(\alpha_3)r_2-\cos\left(\frac{\theta_3}{2}\right)\sin\left(\Theta\right)\xi_{i,j}\sin(\alpha_1)r_2-\sin\left(\frac{\theta_3}{2}\right)\xi_{i,j}\cos\left(\Theta\right)\sin(\alpha_1)r_2$$

$$+\sqrt{3}\sin\left(\frac{\theta_3}{2}\right)\sin\left(\Theta\right)\xi_{i+1,j}\sin(\alpha_4)r_1-\sqrt{3}\cos\left(\frac{\theta_3}{2}\right)\cos\left(\Theta\right)\xi_{i,j}\sin(\alpha_1)r_2+r_2\xi_{i-1,j}\cos\left(\frac{\theta_3}{2}\right)\sin\left(\Theta\right)\sin(\alpha_3)$$

$$-\sin\left(\frac{\theta_3}{2}\right)r_1\xi_{i+1,j}\sin(\alpha_4)\cos\left(\Theta\right)+\sqrt{3}\xi_{i+1,j}\sin(\alpha_4)r_1\cos\left(\frac{\theta_3}{2}\right)\cos\left(\Theta\right)+2r_1r_2\cos\left(\frac{\theta_3}{2}\right)^2-2r_1r_2\sin\left(\frac{\theta_3}{2}\right)^2$$

$$+2\xi_{i+1,j}\cos(\alpha_4)\xi_{i-1,j}\cos(\alpha_3)$$

$$+2\xi_{i+1,j}\sin(\alpha_4)\xi_{i-1,j}\sin(\alpha_3)-2\xi_{i+1,j}\xi_{i,j}\sin(\alpha_4)\sin(\alpha_1)+\sqrt{3}\xi_{i-1,j}\sin(\alpha_3)r_2\cos\left(\frac{\theta_3}{2}\right)\cos\left(\Theta\right)+\sqrt{3}\sin\left(\frac{\theta_3}{2}\right)r_2\xi_{i,j}\sin(\alpha_1)\sin\left(\Theta\right)$$

$$+r_1\cos\left(\frac{\theta_3}{2}\right)\sin(\alpha_4)\sin\left(\Theta\right)\xi_{i+1,j}-\xi_{i,j}\sin(\alpha_1)r_1\cos\left(\frac{\theta_3}{2}\right)\sin\left(\Theta\right)-\sqrt{3}\xi_{i,j}\sin(\alpha_1)r_1\sin\left(\Theta\right)\sin\left(\frac{\theta_3}{2}\right)$$

$$+r_1\xi_{i,j}\sin(\alpha_1)\cos\left(\Theta\right)\sin\left(\frac{\theta_3}{2}\right))\cos\left(\theta_3\right)^3-3\cos\left(\theta_3\right)^2$$

$$-(-2\xi_{i+1,j}\cos(\alpha_4)\xi_{i,j}\cos(\alpha_1)-2\xi_{i-1,j}\sin(\alpha_3)\xi_{i,j}\sin(\alpha_1)+2{\xi_{i,j}}^2-\sqrt{3}r_1\sin\left(\frac{\theta_3}{2}\right)\sin(\alpha_1)\cos\left(\Theta\right)\xi_{i,j}$$

$$-2\xi_{i-1,j}\cos(\alpha_3)\xi_{i,j}\cos(\alpha_1)-\sqrt{3}\sin(\alpha_3)r_2\sin\left(\Theta\right)\sin\left(\frac{\theta_3}{2}\right)\xi_{i-1,j}+\xi_{i-1,j}\sin(\alpha_3)r_2\cos\left(\Theta\right)\sin\left(\frac{\theta_3}{2}\right)$$

$$-\xi_{i,j}\sin(\alpha_1)r_2\cos\left(\frac{\theta_3}{2}\right)\sin\left(\Theta\right)-\xi_{i,j}\sin(\alpha_1)r_2\cos\left(\Theta\right)\sin\left(\frac{\theta_3}{2}\right)$$

$$+\sqrt{3}\xi_{i+1,j}\sin(\alpha_4)r_1\sin\left(\Theta\right)\sin\left(\frac{\theta_3}{2}\right)-\sqrt{3}\xi_{i,j}\sin(\alpha_1)r_2\cos\left(\frac{\theta_3}{2}\right)\cos\left(\Theta\right)+r_2\cos\left(\frac{\theta_3}{2}\right)\sin\left(\Theta\right)\sin(\alpha_3)\xi_{i-1,j}$$

$$-\xi_{i+1,j}\sin(\alpha_4)r_1\cos\left(\Theta\right)\sin\left(\frac{\theta_3}{2}\right)+\sqrt{3}\xi_{i+1,j}\sin(\alpha_4)r_1\cos\left(\Theta\right)\cos\left(\frac{\theta_3}{2}\right)$$

$$+2r_1r_2\cos\left(\frac{\theta_3}{2}\right)^2-2r_1r_2\sin\left(\frac{\theta_3}{2}\right)^2+2\xi_{i+1,j}\cos(\alpha_4)\xi_{i-1,j}\cos(\alpha_3)$$

$$+2\xi_{i+1,j}\sin(\alpha_4)\xi_{i-1,j}\sin(\alpha_3)-2\xi_{i+1,j}\sin(\alpha_4)\xi_{i,j}\sin(\alpha_1)+\sqrt{3}\xi_{i-1,j}\sin(\alpha_3)r_2\cos\left(\frac{\theta_3}{2}\right)\cos\left(\Theta\right)$$

$$+\sqrt{3}\xi_{i,j}\sin(\alpha_1)r_2\sin\left(\Theta\right)\sin\left(\frac{\theta_3}{2}\right)+\sin(\alpha_4)r_1\sin\left(\Theta\right)\cos\left(\frac{\theta_3}{2}\right)\xi_{i+1,j}-\xi_{i,j}\sin(\alpha_1)r_1\sin\left(\Theta\right)\cos\left(\frac{\theta_3}{2}\right)$$

$$-\sqrt{3}\xi_{i,j}\sin(\alpha_1)r_1\sin\left(\Theta\right)\sin\left(\frac{\theta_3}{2}\right)+\xi_{i,j}\sin(\alpha_1)r_1\cos\left(\Theta\right)\sin\left(\frac{\theta_3}{2}\right))2+2))\left(\cos\left(\theta_3\right)\right)$$

$$-(-2\xi_{i+1,j}\cos(\alpha_4)\xi_{i,j}\cos(\alpha_1)-2\xi_{i-1,j}\sin(\alpha_3)\xi_{i,j}\sin(\alpha_1)-\sqrt{3}\xi_{i,j}\sin(\alpha_1)r_1\cos\left(\Theta\right)\cos\left(\frac{\theta_3}{2}\right)-2\xi_{i-1,j}\cos(\alpha_3)\xi_{i,j}\cos(\alpha_1)$$

$$-2r_1r_2-\sqrt{3}\xi_{i-1,j}\sin(\alpha_3)r_2\sin(\Theta)\sin\left(\frac{\theta_3}{2}\right)+\xi_{i-1,j}r_2\sin(\alpha_3)\cos(\Theta)\sin\left(\frac{\theta_3}{2}\right)$$

$$-\xi_{i,j}\sin(\alpha_1)r_2\cos\left(\frac{\theta_3}{2}\right)\sin(\Theta)-\xi_{i,j}\sin(\alpha_1)r_2\sin\left(\frac{\theta_3}{2}\right)\cos(\Theta)\sqrt{3}\xi_{i+1,j}\sin(\alpha_4)r_1\sin(\Theta)\sin\left(\frac{\theta_3}{2}\right)$$

$$-\sqrt{3}\xi_{i,j}\sin(\alpha_1)r_2\cos(\Theta)\cos\left(\frac{\theta_3}{2}\right)$$

$$+\xi_{i-1,j}\sin(\alpha_3)r_2\sin(\Theta)\cos\left(\frac{\theta_3}{2}\right)-\xi_{i+1,j}\sin(\alpha_4)r_1\cos(\Theta)\sin\left(\frac{\theta_3}{2}\right)$$

$$+\sqrt{3}\xi_{i+1,j}\sin(\alpha_4)r_1\cos(\Theta)\cos\left(\frac{\theta_3}{2}\right)+4r_1r_2\cos\left(\frac{\theta_3}{2}\right)^2+2{\xi_{i,j}}^2+2\xi_{i+1,j}\cos(\alpha_4)\xi_{i-1,j}\cos(\alpha_3)$$

$$+2\xi_{i+1,j}\sin(\alpha_3)\xi_{i-1,j}\sin(\alpha_4)-2\xi_{i+1,j}\sin(\alpha_4)\xi_{i,j}\sin(\alpha_1)+\sqrt{3}\xi_{i-1,j}\sin(\alpha_3)r_2\cos(\Theta)\sqrt{3}\xi_{i,j}\cos\left(\frac{\theta_3}{2}\right)\sin(\alpha_1)r_2\sin(\Theta)\sin\left(\frac{\theta_3}{2}\right)$$

$$+\xi_{i+1,j}\sin(\alpha_4)r_1\sin(\Theta)\cos\left(\frac{\theta_3}{2}\right)$$

$$-\xi_{i,j}\sin(\alpha_1)r_1\sin(\Theta)\cos\left(\frac{\theta_3}{2}\right)-r_1\sqrt{3}\xi_{i,j}\sin(\alpha_1)\sin(\Theta)\sin\left(\frac{\theta_3}{2}\right)$$

$$+\xi_{i,j}\sin(\alpha_1)r_1\cos(\Theta)\sin\left(\frac{\theta_3}{2}\right))\left(\sin\left(\theta_3\right)\right))+d\theta_{ij3} \tag{6-A}$$

Variation of inversion angle after buckling:

$$\Delta\beta_{ij}=\frac{1}{3}\left(\Delta\beta_{ij1}+\Delta\beta_{ij2}+\Delta\beta_{ij3}\right)=d\beta_{ij}+\frac{1}{3r_0}\left[\left(\xi_{ij}-\xi_{i-1,j}\right)+\left(\xi_{ij}-\xi_{i+1,j}\right)+\left(\xi_{ij}-\xi_{i,j+1}\right)\right] \tag{7-A}$$

References

[1] T. Chang, H. Gao, Size dependent elastic properties of a single walled carbon nanotube via a molecular mechanics model, J. Mech. Phys. Solids 51 (2003) 1059–1074.
[2] L. Shen, J. Li, Transversely isotropic elastic properties of single-walled carbon nanotubes, Phys. Rev. B 69 (2004), 045414.
[3] J.R. Xiao, B.A. Gama, J.W. Gillespie, An analytical molecular structural mechanics model for the mechanical properties of carbon nanotubes, Int. J. Solids Struct. 42 (2005) 3075–3092.
[4] T. Chang, J. Geng, X. Guo, Chirality- and size-dependent elastic properties of singlewalled carbon nanotubes, Appl. Phys. Lett. 87 (2005), 251929.
[5] T. Chang, W. Guo, X. Guo, Buckling of multi-walled carbon nanotubes under axial compression and bending via a molecular mechanics model, Phys. Rev. B 72 (2005), http://dx.doi.org/10.1103/PhysRevB.72.064101.
[6] C. Li, T.-W. Chou, Modeling of elastic buckling of carbon nanotubes by molecular structural mechanics approach, Mech. Mater. 36 (2004) 1047–1055.
[7] S. Iijima, Helical microtubules of graphitic carbon, Nature 354 (1991) 56–58.
[8] B.I. Yakobson, C.J. Brabec, J. Bernholc, Nanomechanics of carbon tubes: instabilities beyond linear range, Phys. Rev. Lett. 76 (1996) 2511–2514.
[9] C.Q. Ru, Effective bending stiffness of carbon nanotubes, Phys. Rev. B 62 (2000) 9973–9976.
[10] H.S. Shen, Postbuckling prediction of double-walled carbon nanotubes under hydrostatic pressure, Int. J. Solids Struct. 41 (2004) 2643–2657.
[11] N.L. Allinger, Conformational analysis 130: MM2. A hydrocarbon force field utilizing V1 and V2 torsional terms, J. Am. Chem. Soc. 99 (1977) 8127–8134.
[12] U. Burkert, N.L. Allinger, Molecular Mechanics. ACS Monograph 177, American Chemical Society, Washington, DC, 1982.
[13] A.R. Leach, Molecular Modelling Principles and Applications, Addison Wesley Longman Limited, London, 1996, pp. 131–210.
[14] C.T. White, D.H. Robertson, J.W. Mintmire, Helical and rotational symmetries of nanoscale graphatic tubules, Phys. Rev. B 47 (1993) 5485–5488.
[15] A.Y.T. Leung, Y. Wu, W. Zhong, Appl. Phys. Lett 88 (2006), 251908.
[16] C. Li, T.W. Chou, A structural mechanics approach for the analysis of carbon nanotubes, Int. J. Solids Struct. 40 (10) (2003) 2487–2499.
[17] T. Chang, G. Li, X. Guo, Elastic axial buckling of carbon nanotubes via a molecular mechanics model, Carbon 43 (2005) 287–294.
[18] S.C. Fang, W.J. Chang, Y.H. Wang, Computation of chirality- and size-dependent surface Young's moduli for single-walled carbon nanotubes, Phys. Lett. A 371 (2007) 499–503.
[19] Y.Y. Zhang, C.M. Wang, W.H. Duan, Y. Xiang, Z. Zong, Assessment of continuum mechanics models in predicting buckling strains of single-walled carbon nanotubes, Nanotechnology 20 (2009) 8, 395707.
[20] C.F. Cornwell, L.T. Wille, Elastic properties of single-walled carbon nanotubes in compression, Solid State Commun. 101 (1997) 555.
[21] Y. Wang, X.X. Wang, X.G. Ni, H.A. Wu, Simulation of the elastic response and the buckling modes of single-walled carbon nanotubes, Comput. Mater. Sci. 32 (2005) 141–146.
[22] B. Ni, S.B. Sinnott, P.T. Mikulski, J.A. Harrison, Compression of carbon nanotubes filled with C60 CH_4, or Ne: predictions from molecular dynamics simulations, Phys. Rev. Lett. 88 (2005) 2055021.
[23] S.N. Korobeynikov, V.V. Alyokhin, A.V. Babichev, Application of the molecular mechanics method to simulation of buckling of single-walled carbon nanotubes, Eng. Fract. Mech. 130 (2014) 83–95.
[24] Y. Kinoshita, M. Kawachi, T. Matsuura, N. Ohno, Axial buckling behavior of wavy carbon nanotubes: a molecular mechanics study, Phys. E 54 (2013) 308–312.
[25] R. Ansari, H. Rouhi, M. Mirnezhad, A hybrid continuum and molecular mechanics model for axial buckling of chiral single-walled carbon nanotubes, Curr. Appl. Phys. 14 (2014) 1360–1368.
[26] L.C. Zhang, H.S. Shen, Buckling and postbuckling analysis of single-walled carbon nanotubes in thermal environments via molecular dynamics simulation, Carbon 44 (2006) 2608–2616.
[27] M.J. Buehler, Y. Kong, H. Gao, Deformation mechanisms of very long single-wall carbon nanotubes subject to compressive loading, J. Eng. Mater. Technol. 126 (2004) 245.
[28] K.M. Liew, C.H. Wong, X.Q. He, M.J. Tan, S.A. Meguid, Nanomechanics of single and multiwalled carbon nanotubes, Phys. Rev. B 69 (2004) 115429.
[29] H.S. Shen, L.C. Zhang, Postbuckling of double-walled carbon nanotubes with temperature dependent properties and initial defects under combined axial and radial mechanical loads, Int. J. Solids Struct. 44 (2007) 1461–1487.
[30] L. Zhou, B.E. Zhu, Z.Y. Pan, Y.X. Wang, J. Zhu, Reduction of the buckling strength of carbon nanotubes resulting from encapsulation of C60 fullerenes, Nanotechnology 18 (2007) 275709.

[31] A.Y.T. Leung, X. Guo, X.Q. He, H. Jiang, Y.J. Huang, Postbuckling of carbon nanotubes by atomic-scale finite element, Appl. Phys. 99 (2006) 124308.
[32] H. Xin, Q. Han, X.H. Yao, Buckling and axially compressive properties of perfect and defective single-walled carbon nanotubes, Carbon 45 (2007) 2486–2495.
[33] Y.Y. Zhang, V.B.C. Tan, C.M. Wang, Effect of strain rate on the buckling behavior of single- and double-walled carbon nanotubes, Carbon 45 (2007) 514–523.
[34] G.M. Odegard, T.S. Gates, L.M. Nicholson, K.E. Wise, Equivalentcontinuum modeling of nano-structured materials, Compos. Sci.Technol. 62 (14) (2002) 1869–1880.
[35] X. Zhou, J.J. Zhou, Z.C. Ouyang, Strain energy and Young's modulus of single-wall carbon nanotubes calculated from electronic energy-band theory, Phys. Rev. B 62 (20) (2000) 13692–13696.
[36] T. Vodenitcharova, L.C. Zhang, Effective wall thickness of a singlewalled carbon nanotubes, Phys. Rev. B 68 (16) (2003) 165401.
[37] A. Pantano, M.C. Boyce, D.M. Parks, Nonlinear structural mechanics based modeling of carbon nanotube deformation, Phys. Rev. Lett. 91 (2003) 145504.